

pubs.acs.org/cm Methods/Protocols

# Methods for the ICP-OES Analysis of Semiconductor Materials

Calynn Morrison, Haochen Sun, Yuewei Yao, Richard A. Loomis,\* and William E. Buhro\*



Cite This: Chem. Mater. 2020, 32, 1760-1768



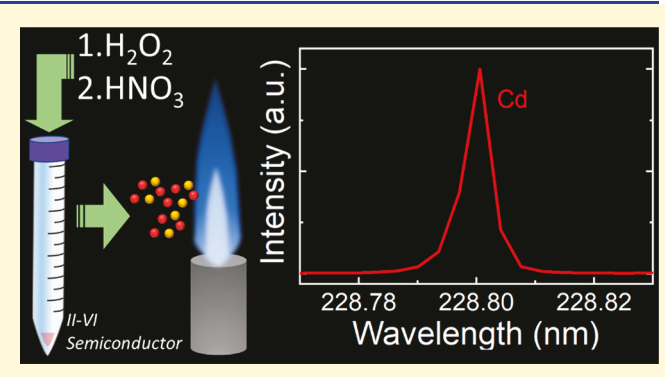
**ACCESS** I

III Metrics & More

Article Recommendations

Supporting Information

ABSTRACT: The techniques employed in the compositional analysis of semiconductor materials by inductively coupled plasma optical emission spectroscopy (ICP-OES) dramatically influence the accuracy and reproducibility of the results. We describe methods for sample preparation, calibration, standard selection, and data collection. Specific protocols are suggested for the analysis of II–VI compounds and nanocrystals containing the elements Zn, Cd, S, Se, and Te. We expect the methods provided will apply more generally to semiconductor materials from other families, such as to III–V and IV–VI nanocrystals.



#### ■ INTRODUCTION

Determination of the stoichiometries of semiconductor nanocrystals is a key aspect of their characterization. Most standard syntheses afford nanocrystals having a superstoichiometric layer of metal cations at their surfaces, such that the metal-to-nonmetal ratio M/E exceeds one. The excess charge from the superstoichiometric cations is counterbalanced by surface-bound anionic ligands. Such nonstoichiometric semiconductor nanocrystals may be interconverted with stoichiometric nanocrystals having charge-neutral surface ligation. Thus, the core stoichiometries of semiconductor nanocrystals are variable and dependent on the surface ligation and nanocrystal size. Understanding and controlling the surface chemistry benefits from the precise determination of nanocrystal core stoichiometry.

Compositional analyses of semiconductor nanocrystals have been conducted by X-ray photoelectron spectroscopy (XPS),<sup>7–10</sup> Rutherford back scattering (RBS),<sup>1,2,7,8,11–13</sup> atomic-absorption spectroscopy,<sup>14</sup> inductively coupled plasma mass spectrometry (ICP-MS),<sup>3,15,16</sup> inductively coupled plasma optical-emission spectroscopy (ICP-OES),<sup>6,15,17,18</sup> X-ray fluorescence spectroscopy (XRF),<sup>19</sup> and energy-dispersive X-ray spectroscopy (EDS) using a transmission electron microscope (TEM).<sup>6</sup> These techniques can be divided into two categories: "beam techniques", which include XPS, RBS, XRF, and EDS, and "digestion-requisite analyses", with ICP-OES, ICP-MS, and flame atomic absorption spectroscopy (FAAS) requiring that samples be digested prior to analysis.

While each analysis method brings advantages and disadvantages, accurate and precise determination of lighter elements or volatile components of semiconducting materials can be challenging regardless of the analytical technique employed. In the case of beam techniques, high-energy photons, electrons, or ions strike the material and may eject

lighter or volatile elements, degrade the surface, or change the oxidation state and crystal structures *during* the measurement. Difficulties determining exact stoichiometries have been reported in XPS, with up to 46% difference between initial and final measurements of metal ions in samples during depth profiling. Some techniques, such as XRF, require that samples must be homogeneous and meet "infinite thickness requirements" in order to produce accurate results. Ligand exchange or surface-chemistry experiments may only result in differences of a single monolayer of atoms between nanostructures, 2,4,12,24 and thus, beam-analysis techniques could yield stoichiometries that deviate from actuality.

Errors in composition similar to those in beam techniques often accompany digestion-requisite techniques. The formation of volatile products of acid digestion results in losses before the measurement. However, by altering the digestion and sample-preparation method, volatile elements and surface components may be retained for measurement, as we demonstrate in this paper. Analyses performed by ICP-OES, ICP-MS, and FAAS are total-composition measurements. Because the samples are digested prior to analysis, particle size or sample thickness is irrelevant. ICP-OES and ICP-MS are capable of detecting concentrations in the parts per million (mg/L) and parts per billion range, respectively. The detection limits for S and Se, for example, may be as low as 0.3 mg/L and 0.2 mg/L, respectively. ICP techniques are

Received: January 20, 2020 Revised: February 21, 2020 Published: February 21, 2020



capable of analyzing upward of 70 elements simultaneously. With multiple emission wavelengths per element, interferences from spectral overlaps can generally be overcome. ICP-OES also offers the convenience to the user of high sample throughput.

In the majority of studies reporting the stoichiometries of semiconductor nanocrystals cited above, the measured M/E ratios have fallen in the range of 1.0-1.8,  $^{1,3,7,9,13,15,16,19}$  and in about a third of these studies the determined values were larger. 6,14,17,18 Interestingly, all but one of these latter studies employed a digestion technique prior to analysis. In the specific case of zinc blende (ZB) CdSe nanoplatelets, fourmonolayer specimens with an expected Cd/Se ratio of 1.25 were analyzed for 1.80  $\pm$  0.07, 15 and five-monolayer specimens with an expected<sup>28</sup> Cd/Se ratio of 1.20 were analyzed for 1.72  $\pm$  0.11, by ICP-OES.<sup>15</sup> (The expected Cd/Se ratios are taken from an analysis of ZB CdS nanoplatelets having the same numbers of monolayers.<sup>28</sup>) While these measured ratios are close to expectation, they are higher, matching the outcomes of most of our initial efforts at ICP-OES analysis. These observations and the experiences conveyed to us by others 29,30 motivated us to conduct a thorough investigation of the ICP-OES analysis of semiconductor materials.

The ICP-OES method detailed in this paper was developed using samples with known or strong theoretical bases for compositions, and protocols were optimized to produce reproducible results that could be compared to the expected values. We report results for four samples of semiconductor nanocrystals, one nanocluster, and one molecular compound as test cases.

We identify several pitfalls associated with conventional ICP-OES analysis. We offer suggestions for improving reproducibility and accuracy in methods for sample digestion, calibration-curve construction, and emission-line and calibration-standard selection. We provide specific protocols for the analysis of compounds and nanocrystals containing cadmium, zinc, sulfur, selenium, and tellurium, which we expect to apply more generally to the analysis of other semiconductor materials, such as InP and PbS. We demonstrate that seemingly small variations in sample preparation, calibration, and data collection can have a large impact on the reliability of the results.

#### MATERIALS

The following nanomaterials were prepared as described in previous reports:  $\{CdSe[n\text{-octylamine}]_{0.53}\}$  quantum belts (QBs),  $^{31}$   $\{CdSe[Cd(oleate)_2]_{0.19}\}$  QBs,  $^{4}$   $[(CdSe)_{13}(n\text{-PrNH}_2)_{13}]$  clusters,  $^{32}$  and  $\{CdTe_{0.50}Se_{0.50}[oleylamine]_x\}$  and  $\{CdTe_{0.73}S_{0.27}[oleylamine]_z\}$  quantum platelets (QPs).

Trace-metal grade nitric acid (70%) and trace-metal grade hydrogen peroxide (32%) were obtained from Millipore Sigma. Zinc diethyldithiocarbamate (97%) was obtained from Sigma-Aldrich. HPLC grade ethanol and methanol were obtained from Sigma-Aldrich. A multielement calibration standard containing Sr, Ba, V, Cr, Co, Ni, Cu, Zn, Mo, Cd, Hg, Pb, U, As, and Se (1000  $\mu$ g/mL) was obtained from Spex Certiprep. A Pure multielement standard containing As and Tl (100  $\mu$ g/mL) and Cd, Pb, and Se (50  $\mu$ g/mL) and a PurePlus multielement standard containing Au, Hf, Ir, Pd, Pt, Rh, Ru, Sb, Sn, and Te (10  $\mu$ g/mL) were obtained from PerkinElmer. Four single-element calibration standards, Cd, Se, Te, and S (1000  $\mu$ g/mL), were obtained from Inorganic Ventures.

Ultrapure water was obtained from a Millipore Direct-Q UV-3 filtration system.

Polypropylene and high-density polyethylene screw-cap centrifuge tubes were obtained from Corning and VWR (Figure S1). The 1000  $\mu$ L solvent-resistant Nichiryo Nichipet EX Plus II and Eppendorf ResearchPlus Micropipettes were employed during ICP-OES sample preparation procedures.

Analyses were conducted using a PerkinElmer ICP-OES PE Optima 7300DV with Syngistix for ICP, Version 2.0.0.22336 software. Detailed instrument settings can be found in Table S1.

#### PROCEDURE

Estimation of Concentration from Synthesis. Analyte solutions were ultimately prepared in the concentration range of 0.5–20 mg/L (see Note S1 in the Supporting Information). This required estimation of the amount of semiconductor compound contained in an analytical sample. We assumed 100% yield in a given semiconductor nanocrystal synthesis, on the basis of the limiting reagent. The following example is given. In a typical synthesis of {CdSe[n-octylamine]<sub>0.53</sub>} quantum belts (QBs), Cd(OAc)<sub>2</sub>·2H<sub>2</sub>O (0.039 g, 1.5 mmol) and selenourea (0.029 g, 2.4 mmol) were allowed to react in noctylamine (3.825 g), making Cd(OAc)<sub>2</sub>·2H<sub>2</sub>O the limiting reagent.<sup>31</sup> The total mass of the crude reaction mixture was 3.893 g.

An aliquot (0.157 g, 200  $\mu$ L) was withdrawn from the reaction mixture, constituting 4% of the mixture and containing 4% of the original cadmium (6.6 × 10<sup>-4</sup> g, 5.8  $\mu$ mol). This aliquot was ultimately digested in hydrogen peroxide (500  $\mu$ L) and nitric acid (500  $\mu$ L) to produce a concentrated digestion solution. The estimated Cd and Se concentrations in this solution were therefore 660 mg/L. As described below, aliquots of the concentrated digestion solution were diluted to 10.00 mL, to produce analytical solutions having Cd-analyte concentrations of 3.3–13.1 mg/L, which were within the desired range for analysis.

General Sample Preparation and Digestion. An aliquot of a nanocrystal dispersion estimated to yield an analyte solution with a final concentration below 20 mg/L (see above) was purified by three centrifugation-washing cycles using centrifugation at 2000 rpm for 3 min, 2 mL of toluene, and a borosilicate test tube in each cycle, each time disposing of the supernatant to remove excess organic material and unreacted precursors. The pellet obtained from the third centrifugation step was then suspended in isopropanol or ethanol, which are solvents compatible with polypropylene and high-density polyethylene (HDPE) centrifuge tubes.<sup>33</sup> The dispersion was transferred to a centrifuge tube and again centrifuged (2000 rpm, 3 min), and the supernatant was removed. The tube was sealed with a rubber septum and dried under vacuum via syringe needle to remove all remaining solvent (Figure S2). A 500 µL aliquot of 30% aqueous hydrogen peroxide solution was added via micropipette, and the centrifuge tube was quickly and tightly closed with a screw cap. The sample was allowed to digest for 3 min, after which the tube was then opened, a 500  $\mu$ L aliquot of 65% aqueous nitric acid solution was added, and the cap was promptly replaced. The reaction mixture was allowed to digest for a minimum of 15 min, until no solid material remained (and the solution had become optically clear and colorless).

Aliquots of the digestion solution containing 200  $\mu$ L, 100  $\mu$ L, and 50  $\mu$ L were pipetted into clean centrifuge tubes and

diluted with a 1% aqueous  $\rm HNO_3$  solution to 10.00 mL, giving analyte solutions with concentrations less than 20 mg/L. The tubes remained tightly capped prior to analysis. Analyses were conducted on the day the analyte solutions were prepared.

**Preparation of Standard Solutions and Construction of the Calibration Lines.** After preparation of the analyte solutions, calibration solutions were prepared using a commercial multielement calibration standard containing 15 elements (Sr, Ba, V, Cr, Co, Ni, Cu, Zn, Mo, Cd, Hg, Pb, U, As, and Se) at concentrations of 1000  $\mu$ g/mL (1000 mg/L). The solutions were prepared in the same PP/HDPE centrifuge tubes mentioned previously. A 200  $\mu$ L micropipette was used to deliver aliquots of the multielement standard in volumes of  $10~\mu$ L,  $20~\mu$ L,  $50~\mu$ L,  $100~\mu$ L, and  $200~\mu$ L and diluted with 1% HNO<sub>3</sub> to a final volume of 10.00 mL using a 10.00 mL pipet. This yielded calibration solutions with concentrations of 1.0, 2.0, 5.0, 10.0, and 20.0 mg/L, respectively.

Emission spectra were collected at the following wavelengths: for Cd, 214.438, 226.502, and 228.802 nm, and for Se, 196.026 and 203.985 nm. The integrated areas of the spectral lines recorded as a function of concentration were then fit to a straight line to obtain the calibration lines for analyte, as discussed below.

Analysis of Experimental Samples. After data collection from the calibration standards, emission spectra were obtained for the experimental analyte solutions at the same wavelengths as used with the standards: for Cd, 214.438, 226.502, and 228.802 nm, and for Se, 196.026 and 203.985 nm. The spectral data were exported, plotted, and inspected for overlapping emission lines. Overlapping emission lines are described in detail in the Results and Discussion portion of this paper.

Figure 1 displays the linear fits obtained from the calibration data for known concentrations of Cd and Se. Integrated

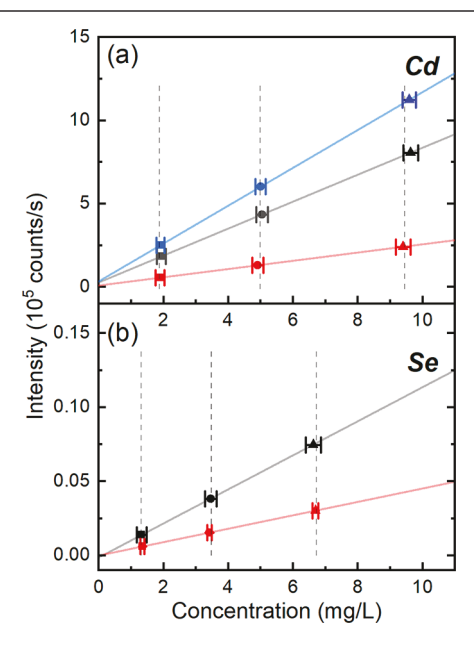


**Figure 1.** ICP-OES calibration lines and data collected from the analysis of  $\{CdSe[n\text{-}octylamine]_{0.53}\}$  QBs. (a) Calibration lines and experimental data points for Cd analyses at the wavelengths 214.438 (red), 226.502 (blue), and 228.802 nm (black); (b) calibration lines and experimental data points for Se analyses at the wavelengths 196.026 (black) and 203.985 nm (red). The dotted lines are averages of the data points at each concentration. Error analysis is described in the Supporting Information.

emission intensities of the spectral lines for digested {CdSe[noctylamine]<sub>0.53</sub>} QBs obtained from three dilutions of experimental analyte solutions are plotted as squares, circles, or triangles on the calibration lines. The concentrations of the experimental analyte solutions in mg/L were determined by plugging the value of the integrated intensity into the linear fit equation and solving for the concentration. The emission lines of Cd at 226.502 nm and Se at 196.026 nm were selected to determine the Cd:Se molar ratios. An example of the conversion of measured mg/L data to a molar ratio is given in eq 1. Error calculations are omitted for clarity. The final ratios reported were averages of those obtained from the various dilutions. An example of the error calculations can be found in Example S1.

$$\frac{1.91 \text{ (mg/L)} \div [112.414 \text{ (g/mol)} \times 1000 \text{ (mg/g)}]}{1.33 \text{ (mg/L)} \div [78.971 \text{ (g/mol)} \times 1000 \text{ (mg/g)}]}$$

$$= 1.01 \text{ Cd:Se}$$
(1)

# SAFETY

Appropriate safety practices for handling strong acids (HNO $_3$ ) and oxidizing agents (H $_2$ O $_2$ ) should be observed. <sup>34</sup> High concentrations of nitric acid and hydrogen peroxide in combination may react violently, producing heat and large volumes of NO $_x$  gas. <sup>35,36</sup> The concentrations used in the digestion procedure here are in the safe range given in ref 29, and we have observed that the combination HNO $_3$  and H $_2$ O $_2$  solutions employed here in the absence of analyte produces only mild bubbling for less than a minute. The safest order of combination is the addition of HNO $_3$ (aq) to H $_2$ O $_2$ (aq), <sup>35</sup> as our procedure does.

Appropriate safety practices for working with nanomaterials and toxic gases should be observed. Particles smaller than 200 nm readily aerosolize when dry. Sample digestion in  $\rm HNO_3/H_2O_2$  may produce volatile, toxic gases such as  $\rm H_2Se$  and  $\rm SO_2$ . Working in a fume hood with proper personal protective equipment mitigates the risk of exposure to both aerosolized and volatile material.

The generation of gas pressure in closed (capped) centrifuge tubes poses a potential problem. The digestion procedure employed here generates sufficient gas pressure to distend a rubber septum cap under the conditions described. The use of HDPE centrifuge tubes mitigates the risks associated with glass; however, caution is advised.<sup>33</sup> HDPE and polypropylene centrifuge tubes are incompatible with toluene and several other aromatic and nonaromatic hydrocarbon solvents.<sup>33</sup> The nanocrystals must be suspended in a compatible solvent like isopropyl alcohol, methanol, or ethanol before transferring them to the HDPE centrifuge tube. If the structure of the tube is weakened due to contact with incompatible solvents, the accumulating pressure from the production of gases becomes a more significant risk. We have not encountered any problems related to overpressurization using the methods described.

# ■ RESULTS AND DISCUSSION

Selection of Standards, Wavelength Selection, and Construction of the Calibration Line. Experiments were conducted using both multielement and single-element standard solutions. The advantages of multielement standards include user convenience, cost savings, and avoidance of error associated with multiple additions to create a custom multielement standard. However, spectral overlaps (of

emission lines) constitute a disadvantage to the use of multielement standards. Cd and As are often present together in commercial multielement standards, despite the overlap of their emission lines at 228.802 and 228.812 nm, as shown in Figure 2a. If such a multielement calibration standard is used, the 228.802 nm line should not be employed for the calibration of Cd due to this overlap.

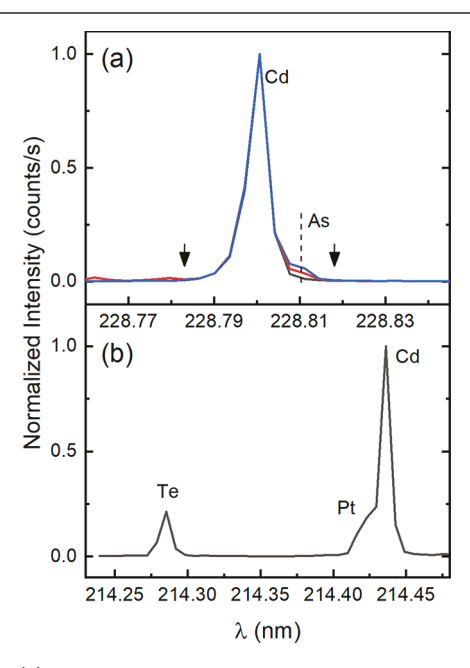


Figure 2. (a) Demonstration of the overlap of the Cd emission at 228.802 nm with the As emission at 228.810 nm (marked by the dotted line). The integration limits are shown by the black arrows (±3.5× the fwhm of the peak). The black spectrum corresponds to a single-element Cd standard. The red spectrum corresponds to a multielement standard having a 1:1 As/Cd ratio (in mg/L units). The blue spectrum corresponds to a multielement standard having a 2:1 As/Cd ratio (in mg/L units). Integration of the Cd emission at 228.802 nm in the multielement standard would result in an overestimation of Cd by 4% and 6%, respectively. (b) Overlap of Pt and Cd emission lines near 214.438 nm, resulting from the combination of multielement calibration standards.

Caution must also be taken when *combining* multielement standards, because of the potential for creating spectrally overlapping emission lines (also referred to here as "spectral overlaps"). For example, multielement standards containing both Cd and Te are not to our knowledge commercially available. Multielement standards containing Te tend to also contain Pt. The combination of such multielement standards containing Cd and Te generates a spectral overlap of Cd and Pt emission lines near 214.438 nm (Figure 2 b). Thus, one could not use the 214.438 nm line to calibrate for Cd concentration with this combination of standard solutions. The emission lines typically used for determination of elements in semiconductor nanocrystals and their potential spectral overlaps are listed in Table 1.

The specific emission lines utilized depend, in part, on the use of commercial or custom multielement calibration solutions. We ultimately prepared custom multielement calibration solutions from single-element standards to avoid spectral overlaps. The Cd emission line at 228.802 nm is generally regarded as reliable for analyses; its high sensitivity allows for detection of ultradilute concentrations.<sup>25</sup> Compar-

Table 1. Commonly Used Emission Lines for Semiconductor Elements and Elements with Potential Overlapping Emission Lines<sup>a</sup>

element	emission $\lambda$ (nm) <sup>27,38</sup>	elements producing potential overlapping emission lines
Al	394.401	U, Ce
	396.152	Mo, Zr, Ce
	167.078	Fe
As	189.042	Cr
	193.696	Ve, Ge
	228.812	Cd, Pt, Ir, Co
Cd	214.438	Pt, Ir
	226.502	Ir
	228.802	Co, Ir, As, Pt
Ge	164.919	Co, Fe, Cu
	219.871	W, Ir, Re, Co
	265.117	Ir, Re
In	158.583	
	230.606	Ni, Os
	325.609	Ir, Re
P	178.287	I
	177.495	Cu, Hf,
	213.618	Cu, Mo
Pb	220.353	Bi, Nb
	217.000	W, Ir, Hf, Sb, Th
S	166.669	Si, B
	180.669	
	181.975	
	182.563	
	189.965	Sn
Se	196.026	Fe
	203.985	Sb, Ir, Cr, Ta
Si	251.611	Ta, U, Zn, Th
	212.412	Hf, Os, Mo, Ta
	288.158	Ta, Ce, Cr, Cd, Th
Sn	189.927	S
	242.170	W, Mo, Rh, Ta, Co
Te	170.000	Sn
	214.281	Ta, Re, V
	225.902	Ir, Os, W, Ga, Ru, Ta
	238.578	Os
Zn	213.856	Ni, Cu, V
	202.548	Nb, Cu, Co, Hf
	206.200	Sb, Ta, Bi, Os
	330.258	Na, Bi, Zr
	334.501	Zr, W

<sup>a</sup>Emission wavelengths and potential overlapping emission lines compiled from refs 31 and 32.

ison of the concentrations obtained using different emission lines, such as 214.438 and 228.802 nm for Cd, afforded a check on the analytical results. In the absence of spectral overlaps, the concentrations found from both lines (measured simultaneously) were within error the same. Note that the determination of apparently different concentrations from two emission lines may indicate the presence of an overlapping line at one or both wavelengths.

We used the emission line at 196.026 nm for Se analyses, although the emission at 203.985 nm was equally usable (Table 1). Zn has five commonly used emission lines; we chose the emission at 206.200 nm for Zn analyses to optimize sensitivity and linearity. In our experience, the S emission lines

at 180.669, 181.975, and 182.563 nm are all suitable for analyses. The S emission at 189.965 nm is too weak for reliable analyses at the concentrations necessary for accurate determinations of Cd and Zn. We used the emission lines at 214.281 and 238.578 nm for Te.

Experiments were conducted to investigate the proper construction of calibration lines. The multielement calibration standard used above, having Cd, Se, Pb, and Zn at 1000 mg/L, was employed to prepare standard solutions at 1 mg/L, 5 mg/L, 10 mg/L, 25 mg/L, and 50 mg/L. Figure 3 below plots the

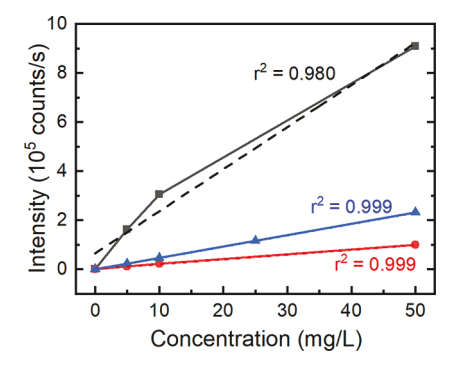


**Figure 3.** Comparison of optical-emission data for Cd (at 228.802 nm, black squares), Zn (at 206.200 nm, red circles), and Pb (at 220.353 nm, blue triangles) over a concentration range of 0–50 mg/L. The solid lines are point-to-point linear segments; the dotted lines (evident only for Cd data) are linear fits to all of the points for each set.

optical-emission intensities for Cd (at 228.802 nm), Zn (at 206.200 nm), and Pb (at 220.353 nm). While the data for Zn and Pb were linear over this range, the Cd data significantly deviated from linearity.

With current instrumentation, users may obtain calibration lines without actual inspection of the data. Use of the linear fit to the Cd data in Figure 3 as a calibration line would lead to errors in determined concentrations as large as 18% (at 25 mg/L). Calibration data may be fit with nonlinear functions; however, training protocols and software packages vary. Nonexpert users will likely find the use of linear calibration fits to be most convenient. This example emphasizes the importance of plotting and inspecting the calibration data at the outset of any experiment.

Additional emission data for Cd collected at three wavelengths are compared in Figure 4. Over the concentration range of 0–100 mg/L (Figure 4a), the data for all three wavelengths, 214.438, 226.502, and 228.802 nm, were nonlinear. However, the data over the lower concentration range of 0–10 mg/L were linear. The results underscore the value of conducting analyses at low concentrations near 10 mg/L. Strong emission lines tend to exhibit nonlinearities in emission intensities at higher concentrations.<sup>25</sup>

The utmost care should be taken in preparation of calibration solutions. Generally, a minimum of 3 (preferably 5) calibration standards should be used per order of magnitude. If the concentration range of samples cannot be estimated in advance of analysis, calibration solutions should be prepared in concentrations scaled by orders of magnitude. With concentration ranges of samples better defined, 3–5 calibration solutions should be prepared with evenly spaced concentrations (5, 10, 15, 20 mg/L, for example). For preparation of calibration solutions within

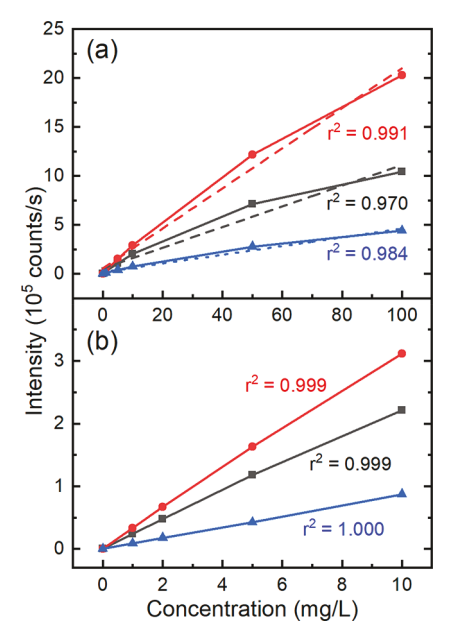


**Figure 4.** Comparison of optical-emission data for Cd at three wavelengths. (a) Emission intensity from Cd at 214.438 nm (blue), 226.502 nm (red), and 228.802 nm (black), over a concentration range of 0–100 mg/L. The linear fits of these data do not produce a satisfactory calibration line. (b) Emission intensity from cadmium at 214.438 nm (blue), 226.502 nm (red), and 228.802 nm (black), over a concentration range of 0–10 mg/L. The solid lines are point-to-point linear segments; the dotted lines are linear fits to all of the points for each set. These linear fits of these data produce a satisfactory calibration line. Errors of the linear fit of (b) are described in Figure S3 in the Supporting Information.

such a narrow concentration range, a single pipet should be used to deliver aliquots of the commercial standard to ensure precision and reproducibility. Calibration solutions over a range of concentrations are sometimes prepared by serial dilutions, which, however, does not ensure higher accuracy than preparing solutions over a concentration range by individual dilutions.<sup>25</sup>

Optimization of Materials and Methods. A series of analyses were conducted on a single synthetic batch of  $\{CdSe[n\text{-}octylamine]_{0.53}\}$  QBs to establish best practices. This material was selected for its stoichiometric wurtzite nanocrystal core having a Cd/Se ratio of unity. Various digestion procedures were conducted in glass and HDPE centrifuge tubes, with the tubes either open or closed during digestion and thereafter. The Cd and Se concentrations in analyte solutions were adjusted to <10 mg/L, within the linear range for both. Calibration data and experimental measurements were obtained from the emission lines at 228.802 nm for Cd and 196.026 nm for Se. The results determined from the different conditions employed are given in Table 2 and Figure 5 and are reported as Cd/Se ratios obtained by the analyses and as deviations from the expected ratio of unity.

The data in Table 2 and Figure 5 establish that generally better results (closer to the expected value of 1) were obtained using HDPE than borosilicate (glass) digestion tubes, especially in closed tubes (with HNO $_3$  or  $H_2O_2/HNO_3$  as digestion agents). The Cd/Se ratios were closer to the theoretical value of unity in HDPE. Because many elements adsorb to the surface of borosilicate glass, Nölte 25 recommends against the use of glass in any phase of the analysis. HDPE

Table 2. Analytical Results Reported as Cd/Se Ratios Obtained from Various Digestion Procedures Using {CdSe[n-octylamine]<sub>0.53</sub>} QBs from a Single Synthetic Batch<sup>a</sup>

HDPE centrifuge tube		borosilicate glass test tube	
open	closed	open	closed
1.046 (4.57%)	1.019 (1.88%)	1.078 (7.84%)	1.096 (9.55%)
1.030 (3.03%)	1.010 (1.00%)	1.019 (1.94%)	1.016 (1.57%)
0.819 (-18.05%)	0.743 (-25.67%)	0.750 (-25.40%)	0.601 (39.87%)
	open 1.046 (4.57%) 1.030 (3.03%)	open         closed           1.046 (4.57%)         1.019 (1.88%)           1.030 (3.03%)         1.010 (1.00%)	open         closed         open           1.046 (4.57%)         1.019 (1.88%)         1.078 (7.84%)           1.030 (3.03%)         1.010 (1.00%)         1.019 (1.94%)

Glass, Open 1 1 Glass, Closed HDPE, Open HDPE Closed Cd/Se Ratio 0.7 0.6 Glass HDPE HDPE Glass HDPF HNO.  $H_2O_2 + HNO_3$ H<sub>2</sub>O<sub>2</sub>

**Figure 5.** Analytical results reported as Cd/Se ratios obtained from various digestion procedures using  $\{CdSe[n-octylamine]_{0.53}\}$  quantum belts from a single synthetic batch. The dashed line is at the expected Cd/Se ratio of unity. The optimal conditions and result are marked by an asterisk. The error bars are plus and minus one standard deviation of the analytical trials.

and/or PP centrifuge tubes are suitable choices during the digestion phase; both materials are resistant to the strong acids and oxidizers used for digestion. It is important to note that HDPE and PP centrifuge tubes are not compatible with all organic solvents.<sup>33</sup> Methanol, ethanol, or isopropanol are good choices for the suspension of nanocrystals for their transfer to the plastic centrifuge tubes.

When the digestions were conducted in HDPE centrifuge tubes, better results (Table 2, Figure 5) were obtained in closed tubes (with HNO3 or H2O2/HNO3 as digestion agents). Semiconductors that generate volatile hydrides, such as H<sub>2</sub>S and H<sub>2</sub>Se, in contact with acid are prone to the loss of these elements during digestion.<sup>25</sup> Such loss leads to the determination of M/S(e) ratios that are higher than those in the analytes and thus to incorrect analytical results. We surmise that similar problems may attend analyses of III-V semiconductors for which digestion may produce PH3 or AsH3. Conducting the digestions in closed containers increases the probability of retention of the volatile species for their oxidation to less volatile solutes. We note that some oxidation products such as SO<sub>2</sub> retain volatility, and so the digestion and analyte solutions should remain in closed containers prior to analyses, which should be completed on the same day. One may also fill the tubes containing analyte solutions such that minimal head space remains open.

Cd/Se ratios were also measured as a function of the digestion agent used. Digestion by HNO<sub>3</sub> in closed HDPE tubes gave Cd/Se ratios close to the expected value (Table 2, Figure 5). However, similar HNO<sub>3</sub> digestions conducted in borosilicate glass produced larger deviations. Digestions conducted with both  $\rm H_2O_2$  and HNO<sub>3</sub> by the procedure

described above gave better results under all circumstances. The use of  $\rm H_2O_2/HNO_3$  in closed HDPE tubes gave the Cd/Se ratio closest to the theoretical and known<sup>4</sup> value of unity for  $\rm \{CdSe[\it{n}\mbox{-}octylamine]_{0.53}\}\ QBs.$ 

Analyses were also conducted using  $H_2O_2$  as the sole digestion agent, for comparison (Table 2, Figure 5). Such digestion is sometimes employed in analyses of biological materials.<sup>39</sup> However, sole use of  $H_2O_2$  for digestion of our samples resulted in very low apparent Cd/Se ratios, indicative of incomplete digestion.

Strong acids such as aqua regia, nitric acid, and concentrated hydrochloric acid are frequently employed for sample digestion prior to ICP-OES analyses. As indicated above, the formation of volatile compounds during digestion can compromise accuracy. Preoxidizing the analyte with  $\rm H_2O_2$  presumably mitigates the formation of  $\rm H_2S$  and  $\rm H_2Se$  upon addition of  $\rm HNO_3$ . The use of an oxidation agent may also promote oxidation by increasing the oxidative power of  $\rm HNO_3$ . We selected  $\rm H_2O_2$  because it is a strong oxidizer in acidic solution  $^{36,40}$  and because high-purity, trace-metal grade >30%  $\rm H_2O_2$  is readily available commercially.

Results from Experimental Specimens. ICP-OES analyses were conducted on several additional specimens from our research program using the optimized procedure described above. The M/E ratios (M = Cd, Zn; E = S, Se, Te, Te + Se, or Te + Se) in the specimens selected were determined from other analytical measurements and from theoretical arguments. Four of the specimens were semiconductor nanocrystals, one was a magic-size nanocluster, and one was a molecular compound. The results are summarized in Table 3.

Table 3. M/E Ratios Determined by Optimized ICP-OES and Other Methods

specimen	M/E <sup>a</sup> ratio from ICP-OES <sup>b</sup>	M/E <sup>a</sup> ratio from other measurements <sup>c</sup>	theoretical
$\{CdSe[n\text{-octylamine}]_{0.53}\}\ QBs$	$1.00 \pm 0.02$	$1.05\pm0.02^{41}$	14
${CdSe[Cd(oleate)_2]_{0.19}}$ QBs	$1.27 \pm 0.02$	$1.19 \pm 0.02$ , $^4 1.21 \pm 0.02$ $^{41}$	1.264
$\{CdTe_{0.50}Se_{0.50}[oleylamine]_x\}$ QPs	$0.98 \pm 0.01$	$1.02 \pm 0.07$	1 <sup>42</sup>
$\{CdTe_{0.73}S_{0.27}[oleylamine]_z\}$ QPs	$1.05 \pm 0.02$	$0.95 \pm 0.06$	1 <sup>42</sup>
$[(CdSe)_{13}(n-PrNH_2)_{13}]$ cluster	$1.00 \pm 0.01$	1.11 <sup>d</sup>	$1^{43}$
$Zn(S_2CNEt_2)_2$	$0.26 \pm 0.02$	0.25 <sup>44</sup>	0.25

 $^{a}$ M = Cd or Zn; E = S, Se, Te, Te + Se, or Te + S.  $^{b}$ The error reported is the propagated error.  $^{c}$ The  $\pm$  values are one standard deviation about the average based on repeated measurements.  $^{d}$ Measurement performed on the analogue [(CdSe)<sub>13</sub>(n-octylamine)<sub>13</sub>] nanocluster.

Table 4.  $\varepsilon$ /Te Ratios ( $\varepsilon$  = Se or S) Determined by ICP-OES and EDS in CdTe-Cd $\varepsilon$  Core-Shell QPs

specimen	$arepsilon/\mathrm{Te}$ ratio from optimized ICP-OES analysis $^a$	$arepsilon/{ m Te}$ ratio from prior ICP-OES analysis $^{26}$	$arepsilon/\mathrm{Te}$ ratio from current EDS analysis $^{arepsilon}$	$\varepsilon/{ m Te}$ ratio from prior EDS analysis $^{26,c}$
$\{CdTe_{0.50}Se_{0.50}[oleylamine]_x\}$	$1.00 \pm 0.01$	0.84 <sup>b</sup>	$0.91 \pm 0.09$	$0.91 \pm 0.06$
$\{CdTe_{0.73}S_{0.27}[oleylamine]_z\}$	$0.39 \pm 0.03$	0.24 <sup>b</sup>	$0.35 \pm 0.05$	$0.32 \pm 0.04$

<sup>&</sup>lt;sup>a</sup>The error reported is the propagated error. <sup>b</sup>Error unavailable. <sup>c</sup>The  $\pm$  values are one standard deviation about the average based on repeated measurements.

The first two specimens in Table 3 are variously ligated CdSe QBs.<sup>4</sup> The wurtzite nanocrystal cores of the {CdSe[n-octylamine]<sub>0.53</sub>} QBs are precisely stoichiometric with Cd/Se ratios of unity, as required by the lack of anions in the empirical formula determined by combustion-based elemental analyses.<sup>4</sup> The average ratio of  $1.05 \pm 0.02$  was determined by repeated energy-dispersive X-ray spectroscopy (EDS) measurements, with a range determined by the standard deviation of those measurements.<sup>41</sup> The ratio of  $1.00 \pm 0.02$  determined by the optimized ICP-OES procedure was very close to the expected, theoretical value of unity. In this case, the error has been propagated through each step of the analysis and includes multiple measurements.

In the second specimen, the L-type n-octylamine ligands on the surface of the  $\{CdSe[n\text{-}octylamine]_{0.53}\}$  QBs were exchanged by Z-type  $Cd(oleate)_2$  ligands to give  $\{CdSe[Cd(oleate)_2]_{0.19}\}$  QBs. As this exchange adds additional Cd atoms to the surface of the quantum belts, the Cd/Se ratio becomes greater than one. The theoretical ratio of 1.26 is the value achieved by coordinating one  $Cd(oleate)_2$  ligand per 3-coordinate surface Se atom. The values derived from combustion-based elemental analysis,  $1.19 \pm 0.02$ , and EDS,  $1.21 \pm 0.02$ , were slightly below the theoretical ratio. The value obtained by the optimized ICP-OES procedure,  $1.27 \pm 0.02$ , was in agreement with theory.

The third and fourth specimens in Table 3 are core—shell CdTe—CdSe and CdTe—CdS QPs. We determined the Cd/E ratios (E = Te + Se or Te + S) in a prior study by EDS and a nonoptimal ICP-OES procedure. Whereas the Cd/E ratios determined by EDS remained close to the expected value of one, those measured by ICP-OES increasingly deviated to larger apparent ratios with increasing CdSe or CdS shell thickness. Additionally, the nonoptimized procedure produced Se/Te and S/Te ratios measured by ICP-OES that were smaller than those determined by EDS.

The differences in the Cd/E ratios measured by EDS and ICP-OES were in the pattern expected for partial loss of volatile S and Se species during preparation of ICP-OES samples. The digestion procedure employed in the prior study<sup>26</sup> differed from the optimized procedure described here. Analytical samples were first digested by HNO<sub>3</sub> and subsequently by HCl in closed, polytetrafluoroethylene

containers. Here we analyzed comparable core—shell CdTe—CdSe and CdTe—CdS nanoplatelets using the optimized procedure.

The results of these new analyses are recorded in Table 3. The Cd/E ratios determined by EDS,  $1.02 \pm 0.07$ , and ICPOES,  $0.98 \pm 0.01$ , for  $\{\text{CdTe}_{0.50}\text{Se}_{0.50}[\text{oleylamine}]_x\}$  were the same within experimental error. Those determined by EDS,  $0.95 \pm 0.06$ , and ICP-OES,  $1.05 \pm 0.02$ , for  $\{\text{CdTe}_{0.73}\text{S}_{0.27}[\text{oleylamine}]_z\}$  may have differed by more than the error in the analyses. The EDS ratio of 0.95 seemed too low, and the ICP-OES ratio of 1.05 seemed too high, given the expected ratio of 1. The empirical formula (and therefore absence of acetate) was not established by combustion-based elemental analysis in this case, 26 and we entertain the possibility that these nanoplatelets may contain excess Cd.

Further validation for the optimized ICP-OES procedure was obtained by comparison of  $\varepsilon$ /Te ratios ( $\varepsilon$  = S or Se) by ICP-OES using the optimized procedure here and for comparable samples analyzed previously<sup>26</sup> by a nonoptimal ICP-OES method and EDS (Table 4). In the prior study, the  $\varepsilon$ /Te ratios measured by ICP-OES were always *smaller* than those measured by EDS, suggesting volatilization of S and Se during ICP-OES analysis. Here the Se/Te ratio determined by ICP-OES, 1.00  $\pm$  0.01, for {CdTe<sub>0.50</sub>Se<sub>0.50</sub>[oleylamine]<sub>x</sub>} was larger than that previously determined for a comparable sample, 0.84, error unavailable. Although the ICP-OES ratio measured here differed from the corresponding Se/Te ratios measured by EDS (Table 4), the values were within experimental error. Here, the S/Te ratio determined by ICP-OES, 0.39  $\pm$  0.03, for {CdTe<sub>0.73</sub>S<sub>0.27</sub>[oleylamine]<sub>z</sub>} QPs was larger than that previously determined for a comparable sample, 0.24, error unavailable, and in close agreement with the values determined by EDS (Table 4). Among the four ratios determined for each of the two specimens, only the ratios measured previously by a nonoptimal ICP-OES analysis differed by more than experimental error. The results establish that the optimized ICP-OES methods described here gave more reliable values and that loss of volatile S and Se species during analysis is the likely cause of the deviation.

Although the emphasis here is on analyses of semiconductor nanocrystals, we included two molecular compounds for comparison, also listed in Table 3. These were analyzed

using the optimized ICP-OES procedure. The first is the magic-size nanocluster  $[(CdSe)_{13}(n-PrNH_2)_{13}]^{.32}$  Here the theoretical or expected Cd/Se ratio of 1 is established by the lack of anions in the empirical formula, as determined by combustion-based elemental analysis and theoretical calculations. At Rutherford backscattering gave a Cd/Se ratio of 1.11 (error unavailable) for the analogue  $[(CdSe)_{13}(n\text{-octylNH}_2)_{13}]$ , and laser-induced-ionization mass spectrometry on this derivative identified the nanocluster core stoichiometry as  $(CdSe)_{13}$ . Here, ICP-OES analysis of  $[(CdSe)_{13}(n\text{-PrNH}_2)_{13}]$  found a Cd/Se ratio of 1.00  $\pm$  0.01, confirming expectation.

Finally, the molecular dithiocarbamate complex Zn- $(S_2CNEt_2)_2$  was analyzed. The theoretical or expected Zn/S ratio of 0.25 was obtained from the empirical formula determined by elemental analysis and X-ray crystallography. The ratio of 0.26  $\pm$  0.02 determined by ICP-OES matched the expected value.

# CONCLUSIONS

Herein we have provided methods and procedures for accurate determination of the composition of semiconductor nanocrystals via ICP-OES. In general terms, we recommend sample digestion in closed, HDPE containers using H<sub>2</sub>O<sub>2</sub> and HNO<sub>3</sub> solutions in sequence. We also advise care in construction of calibration lines and attention to potential spectral overlaps. We also remind researchers that ICP-OES measurements are obtained in units of mg/L (ppm), which must be converted to molarities to determine molar ratios (eq 1). In our experience, if unexpectedly low M/E ratios are determined when compared to other measurements or theoretical calculations, the digestion process is likely incomplete, and the fraction of HNO<sub>3</sub> should be carefully increased. If unexpectedly high M/E ratios are determined, the nonmetallic element E is likely depleted by volatilization. Although we have studied only materials and compounds corresponding to groups II and VI, we expect the methods detailed here to be more broadly applicable.

# ASSOCIATED CONTENT

#### Supporting Information

The Supporting Information is available free of charge at https://pubs.acs.org/doi/10.1021/acs.chemmater.0c00255.

Video of the digestion procedure (MP4)

Photographs of digestion tubes before and in use and a septum-capped polypropylene centrifuge tube under vacuum, instrumentation details, discussion of units, example of a suban example emission spectrum, and a description of error analysis (PDF)

# AUTHOR INFORMATION

#### **Corresponding Authors**

William E. Buhro – Department of Chemistry and Institute of Materials Science and Engineering, Washington University, St. Louis, Missouri 63130-4899, United States; orcid.org/ 0000-0002-7622-4145; Email: buhro@wustl.edu

Richard A. Loomis — Department of Chemistry and Institute of Materials Science and Engineering, Washington University, St. Louis, Missouri 63130-4899, United States; orcid.org/0000-0002-3172-6336; Email: loomis@wustl.edu

#### **Authors**

Calynn Morrison — Department of Chemistry and Institute of Materials Science and Engineering, Washington University, St. Louis, Missouri 63130-4899, United States; orcid.org/0000-0002-0952-3444

Haochen Sun — Department of Chemistry and Institute of Materials Science and Engineering, Washington University, St. Louis, Missouri 63130-4899, United States; orcid.org/0000-0001-7390-843X

Yuewei Yao — Department of Chemistry and Institute of Materials Science and Engineering, Washington University, St. Louis, Missouri 63130-4899, United States; © orcid.org/ 0000-0001-9979-7061

Complete contact information is available at: https://pubs.acs.org/10.1021/acs.chemmater.0c00255

#### Note

The authors declare no competing financial interest.

#### ACKNOWLEDGMENTS

We thank Profs. Volkan Helmi Demir (Bilkent University), Brandi Cossairt (University of Washington), Luisa Whittaker-Brooks (University of Utah), and Dr. Michael Enright (University of Illinois Urbana—Champaign) for helpful discussions. This work was supported by the NSF under Grants DMR-1611149 and DMR-1905751 (R.A.L.) and CHE-1607862 (W.E.B.).

#### REFERENCES

- (1) Taylor, J.; Kippeny, T.; Rosenthal, S. J. Surface Stoichiometry of CdSe Nanocrystals Determined by Rutherford Backscattering Spectroscopy. *J. Cluster Sci.* **2001**, *12* (4), 571–582.
- (2) Anderson, N. C.; Hendricks, M. P.; Choi, J. J.; Owen, J. S. Ligand Exchange and the Stoichiometry of Metal Chalcogenide Nanocrystals: Spectroscopic Observation of Facile Metal-Carboxylate Displacement and Binding. *J. Am. Chem. Soc.* **2013**, *135* (49), 18536–18548.
- (3) Moreels, I.; Lambert, K.; De Muynck, D.; Vanhaecke, F.; Poelman, D.; Martins, J. C.; Allan, G.; Hens, Z. Composition and Size-Dependent Extinction Coefficient of Colloidal PbSe Quantum Dots. *Chem. Mater.* **2007**, *19* (25), 6101–6106.
- (4) Zhou, Y.; Wang, F.; Buhro, W. E. Large Exciton Energy Shifts by Reversible Surface Exchange in 2D II–VI Nanocrystals. *J. Am. Chem. Soc.* **2015**, *137* (48), 15198–15208.
- (5) Luther, J. M.; Pietryga, J. M. Stoichiometry Control in Quantum Dots: A Viable Analog to Impurity Doping of Bulk Materials. *ACS Nano* **2013**, *7* (3), 1845–1849.
- (6) Morris-Cohen, A. J.; Donakowski, M. D.; Knowles, K. E.; Weiss, E. A. The Effect of a Common Purification Procedure on the Chemical Composition of the Surfaces of CdSe Quantum Dots Synthesized with Trioctylphosphine Oxide. *J. Phys. Chem. C* **2010**, 114 (2), 897–906.
- (7) Katari, J. E. B.; Colvin, V. L.; Alivisatos, A. P. X-ray Photoelectron Spectroscopy of CdSe Nanocrystals with Applications to Studies of the Nanocrystal Surface. *J. Phys. Chem.* **1994**, *98* (15), 4109–4117.
- (8) Voznyy, O.; Zhitomirsky, D.; Stadler, P.; Ning, Z.; Hoogland, S.; Sargent, E. H. A Charge-Orbital Balance Picture of Doping in Colloidal Quantum Dot Solids. *ACS Nano* **2012**, *6* (9), 8448–8455.
- (9) Jasieniak, J.; Mulvaney, P. From Cd-Rich to Se-Rich the Manipulation of CdSe Nanocrystal Surface Stoichiometry. *J. Am. Chem. Soc.* **2007**, *129* (10), 2841–2848.
- (10) Peng, Z. A.; Peng, X. Nearly Monodisperse and Shape-Controlled CdSe Nanocrystals via Alternative Routes: Nucleation and Growth. *J. Am. Chem. Soc.* **2002**, *124* (13), 3343–3353.

- (11) Underwood, D. F.; Kippeny, T.; Rosenthal, S. J. Ultrafast Carrier Dynamics in CdSe Nanocrystals Determined by Femtosecond Fluorescence Upconversion Spectroscopy. *J. Phys. Chem. B* **2001**, *105* (2), 436–443.
- (12) Anderson, N. C.; Owen, J. S. Soluble, Chloride-Terminated CdSe Nanocrystals: Ligand Exchange Monitored by <sup>1</sup>H and <sup>31</sup>P NMR Spectroscopy. *Chem. Mater.* **2013**, 25 (1), 69–76.
- (13) Fritzinger, B.; Capek, R. K.; Lambert, K.; Martins, J. C.; Hens, Z. Utilizing Self-Exchange To Address the Binding of Carboxylic Acid Ligands to CdSe Quantum Dots. *J. Am. Chem. Soc.* **2010**, 132 (29), 10195–10201.
- (14) Dai, Q.; Wang, Y.; Li, X.; Zhang, Y.; Pellegrino, D. J.; Zhao, M.; Zou, B.; Seo, J.; Wang, Y.; Yu, W. W. Size-Dependent Composition and Molar Extinction Coefficient of PbSe Semiconductor Nanocrystals. ACS Nano 2009, 3 (6), 1518–1524.
- (15) Yeltik, A.; Delikanli, S.; Olutas, M.; Kelestemur, Y.; Guzelturk, B.; Demir, H. V. Experimental Determination of the Absorption Cross-Section and Molar Extinction Coefficient of Colloidal CdSe Nanoplatelets. *J. Phys. Chem. C* **2015**, *119* (47), 26768–26775.
- (16) Montoro Bustos, A. R.; Encinar, J. R.; Fernández-Argüelles, M. T.; Costa-Fernández, J. M.; Sanz-Medel, A. Elemental Mass Spectrometry: a Powerful Tool for an Accurate Characterisation at Elemental Level of Quantum Dots. *Chem. Commun.* **2009**, No. 21, 3107–3109.
- (17) Hughes, B. K.; Ruddy, D. A.; Blackburn, J. L.; Smith, D. K.; Bergren, M. R.; Nozik, A. J.; Johnson, J. C.; Beard, M. C. Control of PbSe Quantum Dot Surface Chemistry and Photophysics Using an Alkylselenide Ligand. *ACS Nano* **2012**, *6* (6), 5498–5506.
- (18) Morris-Cohen, A. J.; Frederick, M. T.; Lilly, G. D.; McArthur, E. A.; Weiss, E. A. Organic Surfactant-Controlled Composition of the Surfaces of CdSe Quantum Dots. *J. Phys. Chem. Lett.* **2010**, *1* (7), 1078–1081
- (19) Wilcoxon, J. P.; Provencio, P. P. Chemical and Optical Properties of CdSe and CdSe/ZnS Nanocrystals Investigated Using High-Performance Liquid Chromatography. *J. Phys. Chem. B* **2005**, 109 (28), 13461–13471.
- (20) Hoye, R. L. Z.; Brandt, R. E.; Osherov, A.; Stevanović, V.; Stranks, S. D.; Wilson, M. W. B.; Kim, H.; Akey, A. J.; Perkins, J. D.; Kurchin, R. C.; Poindexter, J. R.; Wang, E. N.; Bawendi, M. G.; Bulović, V.; Buonassisi, T. Methylammonium Bismuth Iodide as a Lead-Free, Stable Hybrid Organic—Inorganic Solar Absorber. *Chem. Eur. J.* 2016, 22 (8), 2605–2610.
- (21) Hoye, R. L. Z.; Schulz, P.; Schelhas, L. T.; Holder, A. M.; Stone, K. H.; Perkins, J. D.; Vigil-Fowler, D.; Siol, S.; Scanlon, D. O.; Zakutayev, A.; Walsh, A.; Smith, I. C.; Melot, B. C.; Kurchin, R. C.; Wang, Y.; Shi, J.; Marques, F. C.; Berry, J. J.; Tumas, W.; Lany, S.; Stevanović, V.; Toney, M. F.; Buonassisi, T. Perovskite-Inspired Photovoltaic Materials: Toward Best Practices in Materials Characterization and Calculations. *Chem. Mater.* 2017, 29 (5), 1964–1988.
- (22) Saparov, B.; Hong, F.; Sun, J.-P.; Duan, H.-S.; Meng, W.; Cameron, S.; Hill, I. G.; Yan, Y.; Mitzi, D. B. Thin-Film Preparation and Characterization of Cs<sub>3</sub>Sb<sub>2</sub>I<sub>9</sub>: A Lead-Free Layered Perovskite Semiconductor. *Chem. Mater.* **2015**, 27 (16), 5622–5632.
- (23) XRF Data differences: Quantitative, semi-quantitative, and qualitative data. https://www.bruker.com/products/x-ray-diffraction-and-elemental-analysis/handheld-xrf/xrf-data-primer-quantitative-semi-quantitative-qualitative.html (accessed July 5, 2019).
- (24) Chen, P. E.; Anderson, N. C.; Norman, Z. M.; Owen, J. S. Tight Binding of Carboxylate, Phosphonate, and Carbamate Anions to Stoichiometric CdSe Nanocrystals. *J. Am. Chem. Soc.* **2017**, *139* (8), 3227–3236.
- (25) Nölte, J. ICP Emission Spectrometry: A Practical Guide; Wiley-VCH Verlag GmbH & Co, KGaA: Weinheim, Germany, 2003.
- (26) Sun, H.; Buhro, W. E. Core-Shell Cadmium Telluride Quantum Platelets with Absorptions Spanning the Visible Spectrum. ACS Nano 2019, 13 (6), 6982-6991.
- (27) Interactive Periodic Table; Inorganic Ventures. https://www.inorganicventures.com/periodic-table (accessed June 6, 2019).

- (28) Li, Z.; Qin, H.; Guzun, D.; Benamara, M.; Salamo, G.; Peng, X. Uniform Thickness and Colloidal-Stable CdS Quantum Disks with Tunable Thickness: Synthesis and Properties. *Nano Res.* **2012**, *5* (5), 337–351.
- (29) Cossairt, B. M. Personal Communication. University of Washington, Seattle, WA, 2019.
- (30) Whittaker-Brooks, L. Personal Communication. University of Utah, Salt Lake City, UT, 2019.
- (31) Liu, Y.-H.; Wayman, V. L.; Gibbons, P. C.; Loomis, R. A.; Buhro, W. E. Origin of High Photoluminescence Efficiencies in CdSe Ouantum Belts. *Nano Lett.* **2010**, *10* (1), 352–357.
- (32) Wang, Y.; Liu, Y.-H.; Zhang, Y.; Kowalski, P. J.; Rohrs, H. W.; Buhro, W. E. Preparation of Primary Amine Derivatives of the Magic-Size Nanocluster (CdSe)<sub>13</sub>. *Inorg. Chem.* **2013**, *52* (6), 2933–2938.
- (33) Centrifuge Chemical Resistance Table. *Thermo Fisher Scientific*. http://tools.thermofisher.com/content/sfs/brochures/D20825.pdf (accessed June 30, 2019).
- (34) Prudent Practices in the Laboratory: Handling and Management of Chemical Hazards, updated version. National Research Council, The National Academies Press: Washington, DC, 2011; p 360.
- (35) Nitric Acid with Hydrogen Peroxide Reaction Hazards Technical Data Sheet; Solvay Chemicals Inc. https://www.solvay.com/(accessed June 28, 2019).
- (36) Hatcher, W. H.; MacLauchlan, D. W. Conductivity Data of Aqueous Mixtures of Hydrogen Peroxide and Nitric Acid. *Can. J. Res. Sec. B* **1938**, *16b* (8), 253–259.
- (37) Approaches to Safe Nanotechnology; Department of Health and Human Services, Centers for Disease Control and Prevention, National Institute for Occupational Safety and Health: Washington, DC, 2009; Vol. 2009-125.
- (38) Optima Simutaneous Spectrometers Wavelength Tables; Perkin Elmer Instruments LLC: 2002.
- (39) Sah, R. N.; Miller, R. O. Spontaneous Reaction for Acid Dissolution of Biological Tissues in Closed Vessels. *Anal. Chem.* **1992**, 64 (2), 230–233.
- (40) Luque de Castro, M. D., Luque García, J. L. Techniques and Instrumentation in Analytical Chemistry; Elsevier: Amsterdam, The Netherlands, 2002; Vol. 24.
- (41) Yao, Y.; DeKoster, G. T.; Buhro, W. E. Interchange of L-, Z-, and Bound-Ion-Pair X-Type Ligation on Cadmium Selenide Quantum Belts. *Chem. Mater.* **2019**, *31* (11), 4299–4312.
- (42) Wang, F.; Wang, Y.; Liu, Y.-H.; Morrison, P. J.; Loomis, R. A.; Buhro, W. E. Two-Dimensional Semiconductor Nanocrystals: Properties, Templated Formation, and Magic-Size Nanocluster Intermediates. *Acc. Chem. Res.* **2015**, *48* (1), 13–21.
- (43) Wang, Y.; Liu, Y.-H.; Zhang, Y.; Wang, F.; Kowalski, P. J.; Rohrs, H. W.; Loomis, R. A.; Gross, M. L.; Buhro, W. E. Isolation of the Magic-Size CdSe Nanoclusters [(CdSe)<sub>13</sub>(n-octylamine)<sub>13</sub>] and [(CdSe)<sub>13</sub>(oleylamine)<sub>13</sub>]. *Angew. Chem., Int. Ed.* **2012**, *51* (25), 6154–6157.
- (44) Bonamico, M.; Mazzone, G.; Vaciago, A.; Zambonelli, L. Structural Studies of Metal Dithiocarbamates. III. The Crystal and Molecular Structure of Zinc Diethyldithiocarbamate. *Acta Crystallogr.* **1965**, *19* (6), 898–909.
- (45) Nguyen, K. A.; Day, P. N.; Pachter, R. Understanding Structural and Optical Properties of Nanoscale CdSe Magic-Size Quantum Dots: Insight from Computational Prediction. *J. Phys. Chem. C* **2010**, *114* (39), 16197–16209.